REPORT DOCUMENTATION PAGE

Form Approved
OMB No. 0704-0188

1. REPORT DATE *(DD-MM-YYYY)*	2. REPORT TYPE	3. DATES COVERED *(From - To)*
03-02-2010	Journal Article	

4. TITLE AND SUBTITLE

A Model of High-Pressure Ablative Capillary Discharge for Plasma Thrusters with Capillary Wall Thermal Conduction and Radiation Absorption (Preprint)

5a. CONTRACT NUMBER

5b. GRANT NUMBER

5c. PROGRAM ELEMENT NUMBER

6. AUTHOR(S)
L. Pekker & O. Pekker (ERC)

5d. PROJECT NUMBER

5f. WORK UNIT NUMBER
50260542

7. PERFORMING ORGANIZATION NAME(S) AND ADDRESS(ES)

Air Force Research Laboratory (AFMC)
AFRL/RZSA
10 E. Saturn Blvd.
Edwards AFB CA 93524-7680

8. PERFORMING ORGANIZATION REPORT NUMBER

AFRL-RZ-ED-JA-2010-041

9. SPONSORING / MONITORING AGENCY NAME(S) AND ADDRESS(ES)

Air Force Research Laboratory (AFMC)
AFRL/RZS
5 Pollux Drive
Edwards AFB CA 93524-7048

10. SPONSOR/MONITOR'S ACRONYM(S)

11. SPONSOR/MONITOR'S NUMBER(S)
AFRL-RZ-ED-JA-2010-041

12. DISTRIBUTION / AVAILABILITY STATEMENT

Approved for public release; distribution unlimited (PA #10043).

13. SUPPLEMENTARY NOTES
For publication in the Journal of Propulsion and Power.

14. ABSTRACT
A zero-dimensional time-dependent high-pressure slab capillary discharge model with capillary wall thermal conduction and radiation absorption is presented. The model includes a resistor-inductor-capacitor circuit and a heat-transfer radiation model based on a radiation database constructed using PrismSPEC, a commercially available radiation software, to calculate the radiation heat flux output from a uniform plasma slab. The model also includes a model of the thin transition boundary layer between the uniform plasma core and the ablative capillary walls. This transition boundary layer model is used to obtain the boundary conditions connecting the plasma core parameters with the parameters at the ablative surface to calculate the thermal and radiation heat fluxes at the capillary walls. The radiation wall absorption coefficient is assumed to be a constant independent of wavelength and wall temperature and is an input parameter of the model. The wall thermal conductivity is also assumed to be a constant independent of the wall temperature. Thus, the model self-consistently calculates plasma parameters of the capillary discharge and distribution of wall temperature vs. time. The model is used to model high-pressure ablative capillary discharge for plasma thrusters.

15. SUBJECT TERMS

16. SECURITY CLASSIFICATION OF:			17. LIMITATION OF ABSTRACT	18. NUMBER OF PAGES	19a. NAME OF RESPONSIBLE PERSON
a. REPORT	b. ABSTRACT	c. THIS PAGE			Dr. Andrew Ketsdever
Unclassified	**Unclassified**	**Unclassified**	SAR	17	19b. TELEPHONE NUMBER *(include area code)* N/A

A Model of High-Pressure Ablative Capillary Discharge for Plasma Thrusters with Capillary Wall Thermal Conduction and Radiation Absorption (Preprint)

L. Pekker* and O. Pekker†
ERC Inc., Edwards AFB, CA 93524, USA

A zero-dimensional time-dependent high-pressure slab capillary discharge model with capillary wall thermal conduction and radiation absorption is presented. The model includes a resistor-inductor-capacitor circuit and a heat-transfer radiation model based on a radiation database constructed using PrismSPEC, a commercially available radiation software, to calculate the radiation heat flux output from a uniform plasma slab. The model also includes a model of the thin transition boundary layer between the uniform plasma core and the ablative capillary walls. This transition boundary layer model is used to obtain the boundary conditions connecting the plasma core parameters with the parameters at the ablative surface to calculate the thermal and radiation heat fluxes at the capillary walls. The radiation wall absorption coefficient is assumed to be a constant independent of wavelength and wall temperature and is an input parameter of the model. The wall thermal conductivity is also assumed to be a constant independent of the wall temperature. Thus, the model self-consistently calculates plasma parameters of the capillary discharge and distribution of wall temperature vs. time. The model is used to model high-pressure ablative capillary discharge for plasma thrusters.

Nomenclature

A = average mass of heavy particles (neutrals and ions), au
C = capacitor of electrical circuit, F/m.
C_s = sound speed
C_α = carbon fraction of polyethylene molecule
c_P = specific heat at constant pressure
D_c = slab capillary gap
d = width of the initial wall temperature distribution
end = index denoting condition at the exit plane
F_{rad} = radiation heat flux incident on the transition-boundary layer
H_α = hydrogen fraction of polyethylene molecule
H_w = thickness of the capillary wall
h_{CH} = enthalpy of a CH-molecule to bring it from the capillary wall to the plasma volume
I = discharge current per unit of slab length
k_B = Boltzmann constant
L = inductor of electrical circuit, $H \cdot m$
L_c = capillary length
M_C = mass of a hydrogen atom in atomic units
M_H = mass of a carbon atom mass in atomic units
M_0 = unit of atomic mass
$\hat{n}$ = normalized gas number density, a variable of the Knudsen layer model
n_a = number density of neutral atoms

*Research Scientist, leonid.pekker.ctr@edwards.af.mil
† Contractor, oksana.pekker@gmail.com

n_{CH} = molecular number density of ablated molecules
n_i = ion number density
P = pressure
Q = charge of capacitor, Q/m
R = resistor of electrical circuit, $\Omega \cdot$ m
R_{plasma} = plasma resistance per unit length of the slab in y-direction, $\Omega \cdot$ m
sat = index denoting vapor equilibrium (saturation) conditions
sur = index denoting conditions for ablative wall surface
T = plasma temperature
T_b = maximal wall surface temperature
T_{sur} = temperature of the ablative surface
T_w = wall temperature
t = time
$\hat{u}$ = normalized directed velocity, a variable of the Knudsen layer model
V_T = thermal gas velocity
$\hat{V}$ = normalized thermal velocity, a variable of the Knudsen layer model
x = axis directed across the slab
y = axis directed along the slab
z = axis directed along the capillary
Z = average ion charge state
β = ratio of thermal pressure to magnetic pressure
$\hat{\beta}$ = variable of the Knudsen layer model
Γ_{CH} = molecular ablation/absorption rate
$\Gamma_{CH,max}$ = maximal molecular ablation rate
γ = ratio of specific heats
$\Delta\varepsilon_{\Phi}$ = sum of vaporization, dissociation, ionization and electronic excitation energies per CH molecule
ε_{CH} = internal plasma energy per CH molecule
η = radiation absorption length of the wall material
Θ = energy flux incoming into the capillary wall
κ_w = wall material specific heat
λ_{rad} = radiation mean free path
Π = radiation heat source in the bulk of capillary wall
ρ_w = wall material mass density
σ = electrical conductivity
τ = time step
φ = ionization ratio
χ_w = wall thermal conductivity

I. Introduction

The role of space-based systems for both commercial and government customers continues to evolve, continually providing new requirements for the development of satellite propulsion systems. As it is very efficient (small heat losses through the ablative walls), high-pressure ($5\text{x}10^6$-$5\text{x}10^8$ Pa) ablative capillary discharge is a good candidate for high-power (tens kilowatts) plasma thrusters.

A schematic of a slab capillary discharge thruster is shown in Fig. 1. The discharge maintains a resistive arc through a narrow insulating capillary by the continual ablation of an injected mass or, more commonly, the capillary

wall material as shown in Fig. 1. The ablative capillary discharge can be described via a three-layer configuration. The outermost layer is a solid wall, usually some form of polyethylene, occasionally Teflon or some other insulating material. Material from the wall is evaporated, entering the thin transition boundary layer, where it is dissociated, ionized and heated to plasma temperature. The innermost layer is the plasma core. The closed end of the capillary (left side of Fig. 1) is one electrode; the other electrode (right side of Fig. 1) is an open end through which the plasma can flow and expand. Ohmic heating is responsible for plasma heating, ionization, ablation, and radiation, and radiation. In the model, the sonic condition (*Ma* =1 in Fig. 1) is assumed to exist at the open end of the capillary.

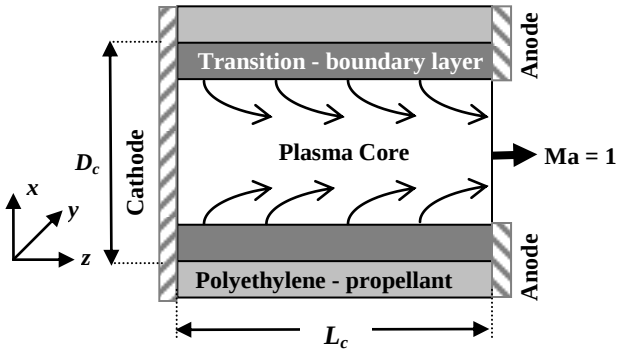

Fig. 1. Schematic (not to scale) of slab capillary discharge operation; (z, x)-cross-section is shown.

As it has been mentioned in [1], in terms of plasma propulsion concepts, the thermal capillary plasma thruster must satisfy two main conditions. First, the capillary plasma should be in a local thermodynamic equilibrium (LTE), indicating that all sorts of particles, electrons, ions, and neutrals have the same temperature. Then, the electrical current will heat both the electrons and the heavy particles (i.e., not only the electrons), thus providing high thrust per watt. Second, as it is well known pinching the capillary discharge leads to a formation of a narrow plasma core region with a high electron temperature and a large, relatively cold peripheral plasma region. This also decreases the efficiency of the capillary thruster, because only a small amount of input discharge energy is transferred to the heavy particles and almost all of the input energy is transferred to the electrons. To minimize the pinching of the capillary discharge, the ratio of the thermal pressure to the magnetic pressure, β, in the capillary plasma thruster should be greater than unity.

The first paper to discuss the use of ablative capillary discharge for propulsion was published in the United States in 1982 [2]. In it, the authors introduced their concept of the pulsed electrothermal thruster; this group later built and tested such devices [3, 4]. Since then many theoretical papers have been published exploring the applications of such discharges to electrothermal capillary thrusters, electrothermal launchers, and electrothermal

chemical guns; a review of these papers with the corresponding references can be found in a recent theoretical paper [1]. It should be noted that in [1] the author for the first time used a radiation heat-transfer model based on a radiation database. This database was constructed using PrismSPECT[‡], a commercially available radiation software that calculates the radiation spectrum output from a uniform plasma slab. Thus, unlike earlier models, this model does not use any asymptotic radiation models, such as blackbody radiation models with a grey factor or volumetric bremsstrahlung (free-free) radiation model, but self-consistently calculates the radiation heat flux at the transition boundary layer, Fig. 1. However, the model [1] neglects the radiation and thermal conduction heating of the bulk capillary wall, assuming that all radiation entering the transition boundary layer is absorbed into this region and expended on the ablation of wall material. On the other hand, as it has been indicated in works [5,6,7] the heat losses in the capillary wall, can play a noticeable role in heat transfer of relatively high-pressure ($2 \cdot 10^5$ - $2 \cdot 10^6$ Pa) capillary discharges. Therefore, extending model [1] to the case of heat transfer in the capillary wall is important to better understand the physics of high-pressure ablative capillary discharge and engineering aspects of the capillary discharge thrusters.

The present paper extends the model [1] to the case of heat transfer in the bulk of capillary wall by taking into account the capillary wall thermal conduction and radiation wall absorption. A description of the model and numerical results are presented in Sections II and III, respectively, and conclusions are given in Section IV.

II. Description of the Model

The following sections describe the assumptions and the model.

A. Assumptions

The following assumptions are made in the model.

1) The boundary transition layer, Fig. 1, is assumed to be thin and is treated in the model as the interface between the plasma core and the capillary wall.

2) The temperatures of electrons and heavy particles (ions and neutrals) are equal, that is, LTE condition is achieved.

3) The magnetic pressure is much smaller than the thermal pressure, that is, $\beta >> 1$.

[‡] Prism Computational Sciences, Inc. 455 Science Drive, Suite 140, Madison, WI 53711.

4) Plasma composition can be calculated using the Saha equation, that is, local plasma-chemistry equilibrium is achieved.

5) The conduction heat flux in the plasma core region is much smaller than the radiation flux at the inner boundary of the transition boundary layer and can be ignored.

6) A sonic condition (Ma = 1 in Fig. 1) at the open end of the capillary.

7) Heating of the plasma by the viscosity drag force is small and can be omitted.

8) The gas in the plasma core region and in the boundary transition layer is fully dissociated.

9) The temperature of the ablative gas entering the plasma core region from the transition boundary layer, Fig. 1, is equal to T , the average temperature of the capillary plasma.

10) The capillary wall is polyethylene, C_4H_9.

11) The capillary is a 4 mm slab.

All eleven of these assumptions have been analyzed in details in [1] and will not be discussed in this paper.

12) Unlike in [1], where the heat losses into the capillary wall were neglected, in this paper we take them into account. We assume that the capillary wall radiation absorption length, η, is a constant, independent of wavelength and wall temperature. This assumption is a stretch because the extinction coefficient of polyethylene is considerably dependent on wavelength [8,9] and temperature. However, since our model is not capable of calculating the radiation spectrum at the capillary wall anyway, and, to the best of our knowledge currently there is no experimental or theoretical data on optical properties of polyethylene as a function of temperature, we have used η as an input parameter.

13) The thermal conduction coefficient of polyethylene is a constant, independent of temperature. In the model all properties of polyethylene materials has been taken from a handbook at room temperature.

In our model we use the radiation-plasma-composition database [1]. This database was constructed using PrismSPECT software for C_4H_9 capillary wall composition and described in detail in [1].

B. Basic equations

The equations describing mass and energy conservation laws in the plasma core region of a slab capillary discharge, Fig. 1, can be written as

$$D_c \cdot L_c \cdot \frac{dn_{CH}}{dt} = 2 \cdot L_c \cdot \Gamma_{CH} - D_c \cdot n_{CH,end} \cdot C_{s,end} \tag{1}$$

$$D_c \cdot L_c \cdot \frac{d(n_{CH} \cdot \varepsilon_{CH})}{dt} = \frac{I^2 \cdot L_c}{D_c \cdot \sigma(n_{CH}, T)} - D_c \cdot n_{CH,end} \cdot C_{s,end} \cdot h_{CH} - 2 \cdot L_c \cdot \Theta \tag{2}$$

where

$$\Theta = \begin{cases} (F_{rad} - \Gamma_{CH} \cdot h_{CH}) & \text{if } F_{rad} > \Gamma_{CH} \cdot h_{CH} \\ 0 & \text{if } F_{rad} < \Gamma_{CH} \cdot h_{CH} \end{cases} \tag{3}$$

$$h_{CH} = \Delta\varepsilon_{\Phi} + c_P \cdot k_B \cdot T \cdot (1 + Z \cdot \varphi) \cdot (C_\alpha + H_\alpha) \tag{4}$$

$$h_{CH} - \varepsilon_{CH} = k_B \cdot T \cdot (1 + Z \cdot \varphi) \cdot (C_\alpha + H_\alpha) \tag{5}$$

$$n_{CH,end} = n_{CH} \cdot \left(\frac{2}{\gamma + 1}\right)^{1/(\gamma - 1)}, \quad T_{end} = \left(\frac{2}{\gamma + 1}\right) \cdot T \tag{6}$$

$$C_{s,end} = \left[\frac{\gamma \cdot k_B \cdot T_{end} \cdot (1 + Z)}{A \cdot M_0}\right]^{1/2}, \quad A = \left(\frac{C_\alpha \cdot M_C + H_\alpha \cdot M_H}{C_\alpha + H_\alpha}\right) \tag{7}$$

$C_\alpha = 4$, $H_\alpha = 9$, $\gamma = 5/3$, $c_P = \gamma/(\gamma - 1)$, and $\varphi = n_i/(n_i + n_a)$ is the ionization ratio; the vaporization and dissociation energies are considered as constants in the model and as input parameters in the code; a detailed explanation of how electron states, plasma conductivity, and plasma composition are calculated are described in [1]; the index "end" denotes conditions at the exit plane and the absence of this index denotes conditions averaged over the volume in the "middle" of capillary. In the model we use isentropic flow relations [10] and assume that the average ion charge and ionization ratio are preserved through the capillary up to the exit plane, $Z_{end} = Z$, and $\varphi_{end} = \varphi$ [1].

In the mass conservation equation, Eq. (1), the first term in the right-hand side describes the number of "CH-polyethylene molecules" arriving to the plasma core region from the ablative surface per unit of time and per unit of the slab length in y-direction, Fig. 1, and the second term is the flow of CH-polyethylene molecules leaving the capillary chamber though the open capillary end per unit of the slab length in y-direction. Factor two in the first term of Eq. (1) corresponds to the two capillary walls in slab geometry. It is worth noting, that the case of $\Gamma_{CH} < 0$ corresponds to the plasma decay case where the particles are absorbed by the capillary wall (not ablated from the wall); in Eq. (1-2) the mass flux is directed to the capillary chamber. In Eq. (2) the first term in the right-hand side is Ohmic heating of the plasma, the second term is enthalpy flow leaving the capillary with the plasma jet through the open capillary end, and the third term is energy losses in the bulk of the capillary wall. It should be stressed that we

assume that the heat flux can be directed only from the plasma to the wall, Eq. (3). This has a perfect physical explanation: in high-pressure capillary discharges the temperature of the plasma core region is always larger than the temperature of the polyethylene capillary which is usually much less than 0.1 eV. As one can see, taking $\Theta = 0$, i.e., no heat losses in the bulk of the capillary wall, we recover model [1].

The heat transfer in the bulk of the capillary wall can be written as

$$\kappa_w \cdot \rho_w \cdot \frac{\partial T_w}{\partial t} - \chi_w \cdot \frac{\partial^2 T_w}{\partial x^2} = \Pi \tag{8}$$

where

$$\Pi = \begin{cases} (1/\eta) \cdot \exp(-x/\eta) \cdot (F_{rad} - \Gamma_{CH} \cdot h_{CH}) & if \ \left(F_{rad} > \Gamma_{CH} \cdot h_{CH}\right) \& \left(\Gamma_{CH} > 0\right) \\ (1/\eta) \cdot \exp(-x/\eta) \cdot F_{rad} & if \ \left(\Gamma_{CH} < 0\right) \\ 0 & if \ \left(F_{rad} < \Gamma_{CH} \cdot h_{CH}\right) \end{cases} \tag{9}$$

The first case in Eq. (9) corresponds to the case of the wall ablation process. In this case the radiation leaving the plasma core region, Fig. 1, ablates the capillary wall, dissociates, ionizes, and heats the ablative vapor up to the plasma temperature; it is then absorbed in the bulk of capillary wall; and finally, it leaves the capillary. The second case corresponds to the plasma decay process, where the mass flux is directed from the capillary chamber to the capillary wall. In this process all the plasma radiation is absorbed by the bulk of capillary wall or leaves the capillary; the enthalpy flux of particles, $\Gamma_{CH} \cdot h_{CH}$, is absorbed by the wall capillary surface and is taken into account in the boundary conditions at the inner surface of the capillary wall, Eq. (20) case 2. The third case in Eq. (9) corresponds to the situation were all radiation incoming into the boundary transition layer from the plasma core region is absorbed in it and expended for ablation of the wall, the case of no heat looses in the bulk of the capillary wall.

It should be stressed that in our model we do not take into account the change in the slab gap, D_c, during the discharge: the slab gap in our radiation database is assumed to be constant and cannot be varied. This limitation is not critical for short pulse capillary discharges; in our calculation the increase in the D_c was about a few microns. However, for long pulse discharges the effect of changing the capillary radius due to ablation has to be taken into account.

In the model we employed the resistor-inductor-capacitor circuit, Fig. 2, to self-consistently calculate the parameters of the capillary discharge and the temperature distribution in the capillary walls vs. time. The equation describing the circuit can be written as

$$\frac{Q}{C} = -L \cdot \frac{d^2 Q}{dt^2} - \left(R_{plasma} + R\right) \cdot \frac{dQ}{dt} \tag{10}$$

The initial parameters for this circuit are initial capacitor voltage and initial circuit current $I = dQ/dt$.

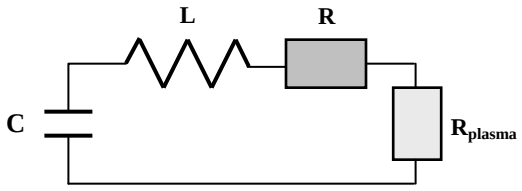

Fig. 2 RLC circuit for modeling capillary discharge.

C. Boundary conditions

Boundary conditions connecting the plasma core parameters with the parameters at the ablative surface are as follows:

$$\Gamma_{CH} = n_{CH,sat}(T_{sur}) \cdot V_{T,sur} \cdot \hat{n} \cdot \hat{u} \tag{11}$$

$$P(n_{CH}, T) = P_{sat}(T_{sur}) \cdot \hat{n} \cdot \left(\frac{\hat{V}^2}{2} + \hat{u}^2 \right) \tag{12}$$

$$\frac{1}{2 \cdot \sqrt{\pi}} = \hat{n} \cdot \hat{u} \left(1 + \hat{\beta} \cdot \left[\frac{\hat{u}}{2} \cdot erfc\left(\frac{\hat{u}}{\hat{V}} \right) - \frac{\hat{V}}{2 \cdot \sqrt{\pi}} \cdot \exp\left(-\frac{\hat{u}^2}{\hat{V}^2} \right) \right] \right) \tag{13}$$

$$\frac{1}{4} = \hat{n} \cdot \left(\frac{\hat{V}^2}{2} + \hat{u}^2 \right) - \hat{n} \cdot \hat{\beta} \cdot \left(\left[\frac{\hat{u}^2}{2} + \frac{\hat{V}^2}{4} \right] \cdot erfc\left(\frac{\hat{u}}{\hat{V}} \right) - \frac{\hat{V} \cdot \hat{u}}{2 \cdot \sqrt{\pi}} \cdot \exp\left(-\frac{\hat{u}^2}{\hat{V}^2} \right) \right) \tag{14}$$

$$\frac{1}{\sqrt{\pi}} = \hat{n} \cdot \hat{u} \cdot \left(\frac{5 \cdot \hat{V}^2}{2} + \hat{u}^2 \right) - \hat{n} \cdot \hat{\beta} \cdot \hat{V}^3 \cdot \left(\frac{1}{2 \cdot \sqrt{\pi}} \cdot \left[\frac{\hat{u}^2}{\hat{V}^2} + 2 \right] \cdot \exp\left(-\frac{\hat{u}^2}{\hat{V}^2} \right) - \frac{\hat{u}}{2 \cdot \hat{V}} \cdot \left(\frac{5}{2} + \frac{\hat{u}^2}{\hat{V}^2} \right) erfc\left(\frac{\hat{u}}{\hat{V}} \right) \right) \tag{15}$$

where Eq. (11) calculates the flux of the ablative polyethylene molecules; Eq. (12) states that the pressure in the plasma core is equal to the vapor pressure in the Knudsen layer at the ablative surface (the Knudsen layer is a part of the transition layer); and Eqs. (13) – (15) describe the Knudsen layer at the ablative surface using Anisimov's velocity distribution function [11]; here we have adopted the Knudsen layer model [12]. In the model we use the following expressions for the equilibrium polyethylene vapor pressure P_{sat} [6], thermal velocity of the evaporated atoms $V_{T,sur}$, and density $n_{CH,sat}$,

$$P_{sat} = \exp\left[5565.22 \cdot \left(\frac{1}{453} - \frac{1}{T_{sur}} \right) \right] \tag{16}$$

$$V_{T,sur} = \sqrt{\frac{2 \cdot k_B \cdot T_{sur}}{M_0 \cdot A}} \tag{17}$$

$$n_{CH,sat} = \frac{P_{sat}}{k_B \cdot T_{sur} \cdot (C_\alpha + H_\alpha)} \tag{18}$$

In Eq. (18) we have assumed that all vapor leaving the ablative surface is fully dissociated. It is worth noting that in this Knudsen layer model, we ignore the thermal conductivity in the Knudsen layer, assuming that radiation heat flux at the ablative surface is much larger than thermal conduction [13]. Indeed, since in the model we assume that the radiation heat flux at the inner boundary of the transition layer is much larger than the conduction heat flux in the plasma core region (assumption 5) the conduction heat flux in the Knudsen is small and can be dropped from the consideration.

Boundary conditions at the outer and inner boundaries of the capillary walls are

$$\left.\frac{\partial T_w}{\partial x}\right|_{H_w} = 0 \tag{19}$$

$$\begin{cases} \left.\dfrac{\partial T_w}{\partial x}\right|_{x_{sur}} = 0 & if\ (\Theta > 0)\ \&\ (\Gamma_{CH} > 0) \\ \left.\dfrac{\partial T_w}{\partial x}\right|_{x_{sur}} = \dfrac{\Gamma_{CH} \cdot h_{CH}}{\chi_w} & if\ (\Theta > 0)\ \&\ (\Gamma_{CH} < 0) \\ T_{sur} = T_b & if\ \Theta = 0 \end{cases} \tag{20}$$

where $x_{sur} = 0$ and $x = H_w$ are the coordinates of the inner and outer boundaries of the capillary walls. Eq. (19) specifies no conduction heat flux at the outer boundary of the capillary wall. The first case in Eq. (20) specifies no conduction heat flux at the inner boundary of the capillary wall in the wall ablation regime. The second case corresponds to the absorption wall regime, the regime in which the mass flux is directed from the plasma to the capillary walls. In this regime the incident particles bring their enthalpy to the capillary wall surface, inducing the corresponding conduction heat flux at the capillary wall. The third case specifies the surface wall temperature as a maximum wall temperature T_b that can provide the maximum ablation rate due to radiation:

$$\Gamma_{CH,\max} = \frac{F_{rad}}{h_{CH}} \tag{21}$$

Thus, Eq. (20) as well as Eqs. (3) and. (9), state that heat flux can be directed only from the plasma to the wall and, therefore,

$$\Gamma_{CH} \le \Gamma_{CH,\max} \tag{22}$$

D. Algorithm

Let us now describe the algorithm for calculating capillary discharge parameters and the temperature distribution in the capillary wall.

1) Assume initial values of n_{CH}, and T, and T_w(x), I, and, and Q.

2) Calculate all plasma parameters for given n_{CH}, and T.

3) Calculate $\Gamma_{CH,max}$ using Eq. (21).

4) Calculate the maximum allowed wall surface temperature T_b by substituting $\Gamma_{CH,max}$ and $P(n_{CH},T)$ into the system of Eqs. (11) – (15).

5) Calculate Γ_{CH} by substituting P(n_{CH},T) and $T_w(x_{sur})$ into the system of Eqs. (11) – (15).

6) Determine the boundary conditions at $x = x_{sur}$, Eq. (20):

6a. if ($T_w(x_{sur}) < T_b$) & ($\Gamma_{CH} > 0$) then apply case 1;

6b. if ($T_w(x_{sur}) < T_b$) & ($\Gamma_{CH} < 0$) then apply case 2;

6c. if $T_w(x_{sur}) > T_b$ then apply case 3 and set Γ_{CH} equal to $\Gamma_{CH,max}$;

7) Calculate new time: $t = t + \tau$, where t is the initial time and τ is the time step.

8) Calculate new n_{CH}, and T by solving Eq. (1) and (2):

$$n_{CH}^{t+\tau} = n_{CH}^{t} + \tau \cdot \left[\frac{2 \cdot \Gamma_{CH}}{D_c} - \frac{n_{CH,end} \cdot C_{s,end}}{L_c} \right]^t \tag{23}$$

$$n_{CH}^{t+\tau} \cdot \varepsilon_{CH}(n_{CH}^{t+\tau}, T^{t+\tau}) = \\ = n_{CH}^{t} \cdot \varepsilon_{CH}(n_{CH}^{t}, T^{t}) + \tau \cdot \left[\frac{I^2}{D_a^2 \cdot \sigma(n_{CH}, T)} - \frac{n_{CH,end} \cdot C_{s,end} \cdot h_{CH}}{L_c} - 2 \cdot \Theta \right]^t \tag{24}$$

9) Calculate new $T_w(x)$ by solving Eq. (8) with boundary conditions (20).

10) Calculate new Q and I solving Eq. (10):

$$Q^{t+\tau} = Q^{t} - I^{t} \cdot \tau \tag{25}$$

$$I^{t+\tau} = I^{t} \cdot \left(1 - \tau \cdot \frac{(R_{plasma} + R)}{L} \right) + \tau \cdot \frac{Q^t}{C \cdot L} \tag{26}$$

11) Go to step 1.

In this work, we have used: the iteration-divide-segment-by-two-method to solve Eq. (24) and the system of Eq. (11) – (15); a standard implicit scheme to solve Eq. (8); and a non-uniform geometric-progression grid.

III. Numerical results

In the numerical results presented in this section, the combined energy of evaporation and dissociation was taken as 50 eV per C_4-H_9 polyethylene molecule, the capillary length was chosen as 8 cm, D_c was 4 mm, the parameters of circuit were $L = 4.661 \cdot 10^{-8}$ H · m, $R = 1.4546\ \Omega \cdot$ m, $C = 1.7507$ F/m, Fig. 2, the initial voltage on the capacitor and the initial discharge current were 2500 V and $1.496 \cdot 10^5$ A/m respectively. The initial temperature distribution of the wall was chosen as,

$$T_w(x) = (527.56 - 300.0) \cdot \frac{Exp[-(x/\eta)^2]}{1 - Exp[-(H_w/\eta)^2]} + \frac{300.0 - 527.56 \cdot Exp[-(H_w/\eta)^2]}{1 - Exp[-(H_w/\eta)^2]} \tag{27}$$

where $x = 0$ corresponds to the ablative surface, $x = H_w$ to the outer boundary of the capillary wall, and the initial parameters of the plasma core were chosen as $n_{CH} = 1.714 \cdot 10^{23}$ m^{-3} and $T = 1.2555$ eV. Thus, in our calculations the width of the initial wall temperature distribution d is on the order of radiation absorption length of the wall material that has a perfect physical sense; than larger η than more deeply radiation penetrates into the capillary wall. To investigate how the radiation absorption of the wall affects the capillary discharge we performed calculations for $\eta =$

0.02, 0.1, and 0.5 mm. It is worth noting, that the selected initial n_{CH} , T, and I correspond to the parameters of the stationary capillary discharge with no heat losses in the bulk of the capillary walls.

Figures 3-4 show the distributions of the LTE parameter [1] (which is the ratio of the average exchange energy between the electrons and the heavy particles due to their collisions to the average energy that an electron gains from the electric field between collisions) and β vs. time for different η. As one can see, these parameters are much larger then one; meaning that assumptions 2 and 3 are well satisfied in our calculations. In the model we have also checked assumptions 4, 5, and 7 employing the methods [1]; they were also well satisfied in our calculations.

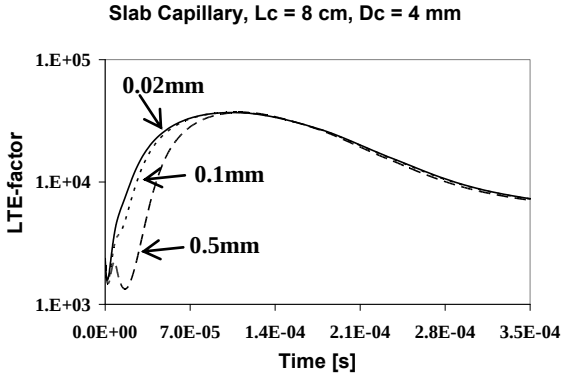

Fig. 3. LTE-factor for different η.

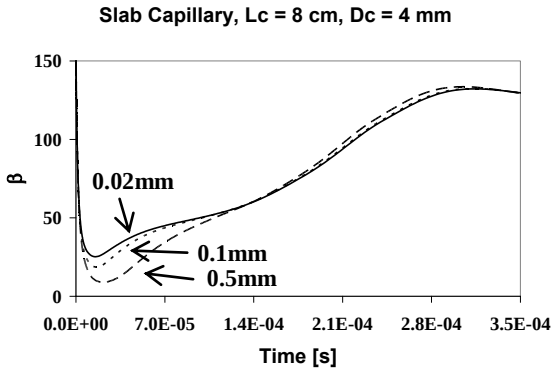

Fig. 4. Ratio of thermal pressure to magnetic pressure for different η.

Now let us analyze Figures 5-10. It is obvious that as the radiation wall absorption length η increases, the temperature of the ablative surface decreases, as shown at the positive slopes of T_{sur} in Fig. 5, leading to a smaller vaporization rate of the wall material. This results in smaller plasma densities and a correspondingly smaller plasma pressure for larger η, as shown in Figs. 6 and 7, but in larger plasma temperatures due to the Ohmic plasma heating (Fig. 8). On the other hand, because of the highly nonlinear dependence of the plasma electrical resistivity on the plasma temperature and plasma composition, the discharge current does not exhibit a significant dependence on η, as shown in Fig. 9; however, it is clear that with an increase in η, the peak current rises. The dip in n_{CH} and the peak in T at the early stage of the discharge seen in Figs. 6 and 8 can be explained by a large imbalance between the ablation, rapid Ohmic heating, and plasma exhaust through the open capillary end at the initial stage of the capillary discharge development; the characteristic time of this stage can be estimated as a few L_c/C_s , which translates to about 20-30 microseconds in our case, Figs. 6 and 8.

At the negative slopes of T_{sur}, Fig. 5, all parameters of the discharge become weakly dependent of η, Figs. 3-9. This observation can be explained by the fact that when T_{sur} decreases with time the heat losses in the bulk of the capillary wall become to be equal to zero in the model, Fig. 10, and, therefore, the parameters of the discharge become weakly dependent of η. Fig. 10 also demonstrates that the energy losses in the capillary bulk dramatically increase with an increase in the radiation wall absorption length, as of course we expect.

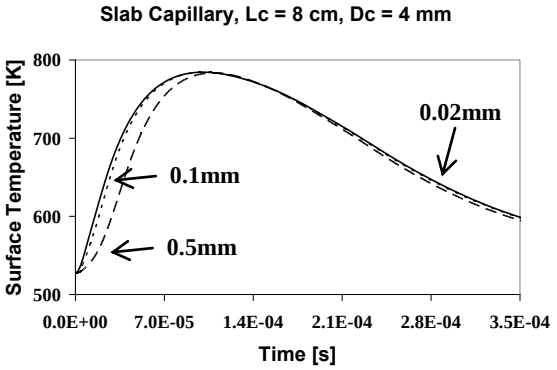

Fig. 5. Temperature of ablative surface for different η.

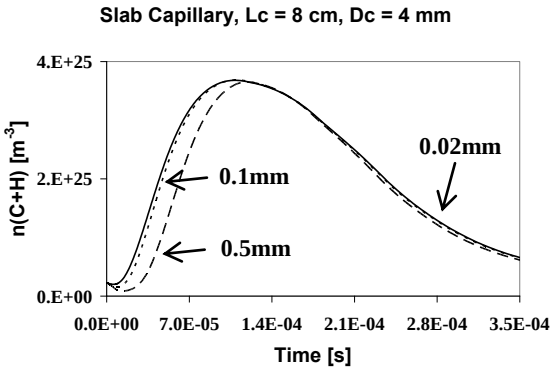

Fig. 6. Number density of heavy particles for different η.

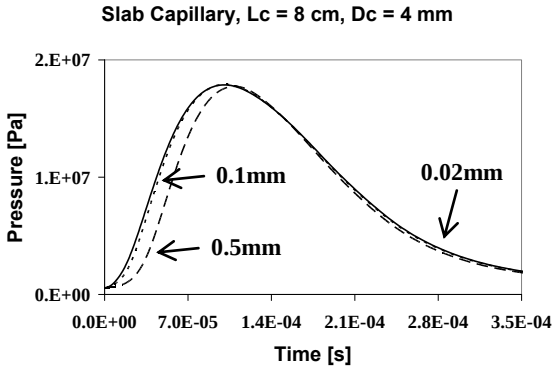

Fig. 7. Plasma pressure for different η.

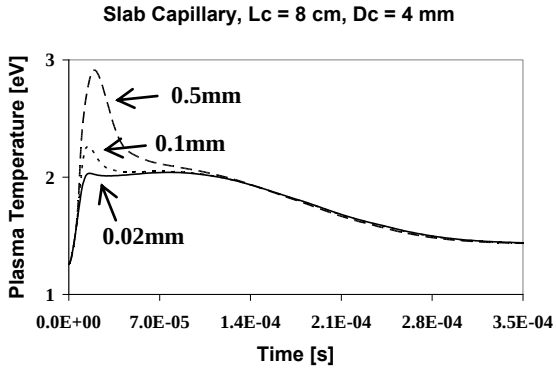

Fig. 8. Plasma temperature for different η.

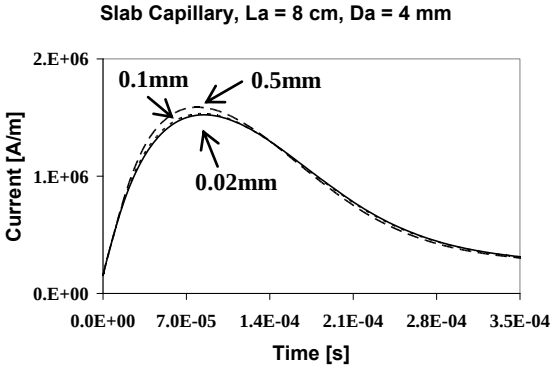

Fig. 9. Discharge current for different η.

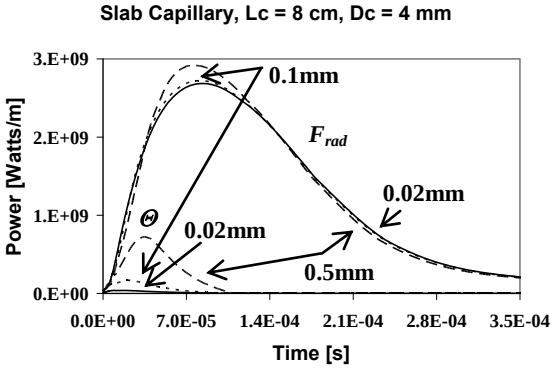

Fig. 10. F_{rad} and Θ for different η.

Figs. 11 - 13 illustrate wall temperature distributions at different moments of time and for different η. Since the thermal conductivity of the polyethylene is small, the characteristic widths of the temperature distributions depend on η. However, when the ablative surface is cooled by the vaporization process, the length of the positive temperature slopes depends on χ_w.

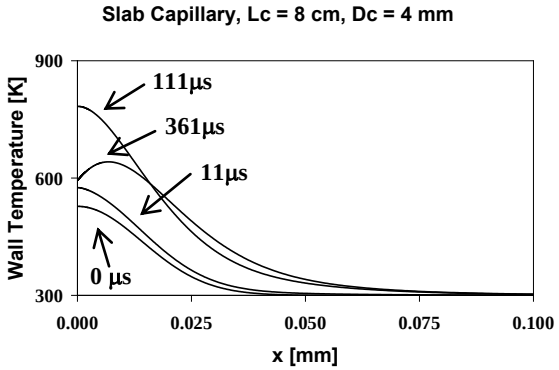

Fig. 11. Wall temperature distribution for η = 0.02 mm at different moments of time.

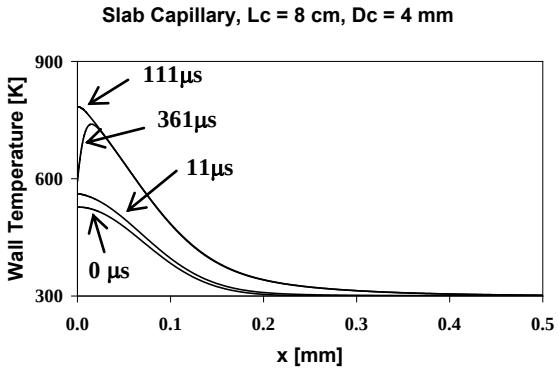

Fig. 12. Wall temperature distribution for η = 0.1 mm at different moments of time.

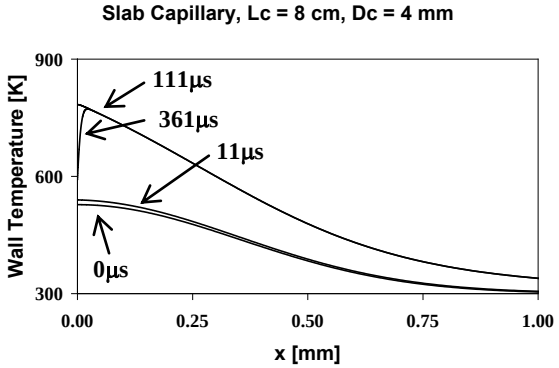

Fig. 13. Wall temperature distribution for η = 0.5 mm at different moments of time.

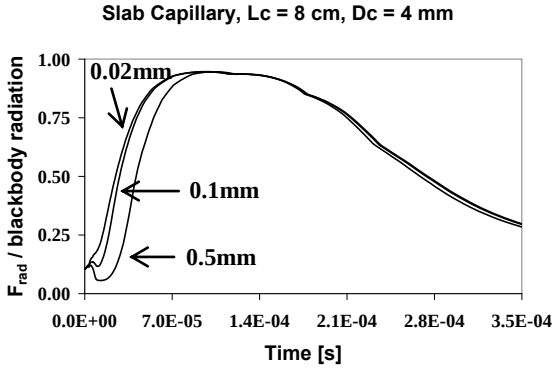

Fig. 14. Grey factor for different η.

Fig. 14 shows the ratio of the calculated radiation flux at the transition boundary layer, Fig. 1, to the blackbody radiation flux with the same plasma temperature, that is, the grey factor. As one can see the grey factor varies from 0.06 to 0.95. This illustrates that the grey factor can change significantly with time in a non-steady operation regime and, therefore, assuming that it is constant can lead to false results.

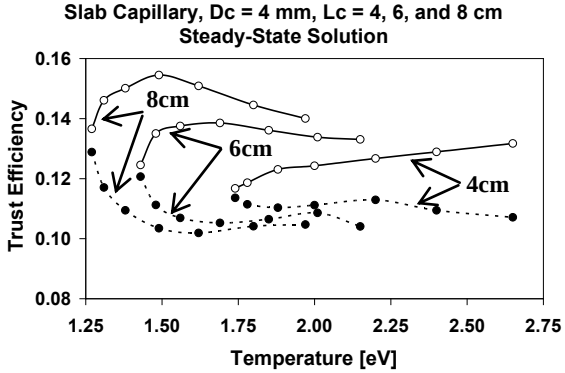

Fig. 15. Thrust efficiency for different L_c; dashed line: MHP regime, solid SHP regime.

One of the most important parameters of thruster performance is the thrust efficiency, how much of the energy deposited or stored in the propellant is actually transferred into the kinetic energy of the gas/plasma leaving the rocket. Fig. 15 shows the thrust efficiency calculated for the steady-state capillary discharge regime for different capillary lengths. In these calculations we have assumed no heat losses from the capillary walls and the energy of evaporation and dissociation have been taken as zero (for polyethylene they are much smaller than the ionization potential of carbon and hydrogen and because the ionization ratio of the plasma in these stationary regimes are larger than 15% [1] they can be ignored). As shown in Fig. 15, the model gives two steady-state solutions at the given plasma temperature [1]. The first solution corresponds to the regime superhigh-pressure (SHP) [1] in which the plasma is so dense that the radiation mean free path, λ_{rad}, is less than the slab gap of the capillary. The second regime occurs when the plasma density is much lower, so that $\lambda_{rad} >> D_c$, that is the case of moderately high plasma pressure, MHP regime. Detailed discussion of steady state solutions and results can be found in [1]. As one can see at a given plasma temperature in the SHP regime the thrust efficiency increases with capillary length and in MHP regime decreases. An explanation of this observation as follows.

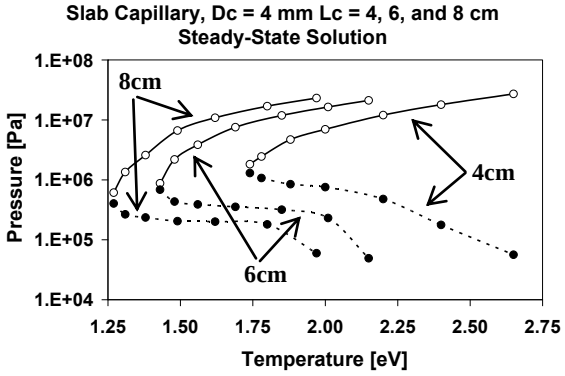

Fig. 16. Plasma Pressure for different L_c; dashed line: MHP regime, solid SHP

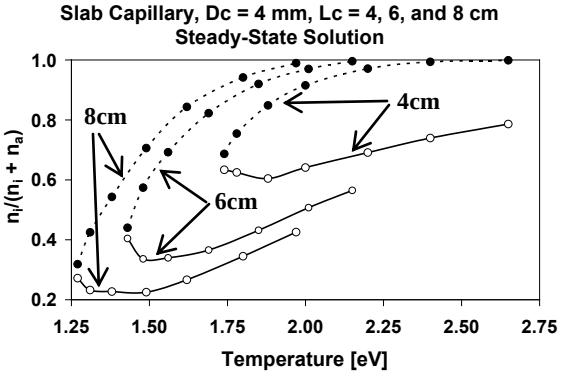

Fig. 17. Ionization ratio for different L_c; dashed line: MHP regime, solid SHP regime.

In high-pressure capillary discharges with plasma temperatures of a few electron volts, the main part of electrical energy deposited in the discharge is spent on ionization of the vapor arriving into the plasma core, Fig. 1. Since the ionization ratio decreases with an increase in the plasma pressure (this follows from Saha equation), the ratio of energy contribution in ionization of the vapor arriving in the plasma chamber, Fig. 1, to the total energy spent on the vapor heating up to plasma temperature decrease with an increase in the plasma pressure. As follows from Figs. 16 and 17, at a given plasma temperature for SHR regime of operation, the plasma pressure increases and correspondingly the ionization ratio decreases with an increase in the capillary length, while the plasma pressure decreases and ionization ratio increases in MHP regimes. Thus, since the main part of enthalpy leaving the capillary with the plasma jet is in ionization, the thrust efficiency decreases with an increase in the ionization ratio that explains Fig. 15.

The fact that the main part of plasma enthalpy is in "ionization energy", not in thermal energy of the plasma, explains why the thrust efficiency of high-pressure capillary discharge does not exceed 20%, Fig. 15. Using a nozzle

may significantly improve the performance of capillary thrusters by conversion of the thermal and chemical energies of the plasma leaving the capillary into kinetic energy of the plasma jet, as in ordinary chemical rockets.

IV. Conclusions

We have presented a zero-dimensional model of high-pressure slab capillary discharge model with capillary wall thermal conduction and radiation absorption. The model includes: a heat-radiation model based on radiation database to self-consistently calculate the radiation flux at the thin transition boundary layer between the uniform plasma core and the ablative surface; a model of the transition boundary layer to obtain the boundary conditions connecting the plasma core parameters with the parameters at the ablative surface; and the resistor-inductor-capacitor circuit. Thus, the model allows the self-consistent calculation of plasma parameters and distribution of wall temperature vs. time. The radiation wall absorption coefficient is assumed to be constant and is an input parameter of the model. The last assumption is a stretch because the extinction coefficient of polyethylene is considerably dependent on wavelength and temperature which may change significantly in the course of discharge. Since the model is not capable of calculating the radiation spectrum at the ablative surface anyway, this is the extend of what the model is capable of.

Our model shows that small extinction coefficient of the wall material lead to large energy losses from the capillary discharges (the heat is absorbed by the bulk of the capillary wall or just escapes the capillary), to a spike in the plasma temperature. If the extinction coefficient is too small, the discharge may become extinguished because the temperature of ablative surface does not increase fast enough to compensate the plasma exhaust from the open end of the capillary, Fig. 1. Thus, for thruster applications the capillary wall material has to have the radiation absorption coefficient as large as possible to improve the energy efficiency of the thruster and that also helps to easier achieve stable regimes of thruster operation.

The model also indicates that despite the fact that thrust efficiency of the high-pressure capillary discharge thruster is rather small, likewise in all thermal thrusters at high temperatures, its performance can be significantly improved by using a nozzle, as in conventional chemical rockets.

Acknowledgments

The authors would like to thank M. P. Young and A. P. Pancotti for helpful discussions, and their gratitude to A. Pekker and M. Kapper for their kind help in preparing the text of this paper.

References

[1] Pekker, L., "A Zero Dimensional Time-Dependent Model of High-Pressure Ablative Capillary Discharge," Journal of Propulsion and Power, Vol. 25, No. 4, 2009, pp. 958-969.

[2] Burton, R. L., Goldstein, S. A., Tidman, D. A., and Winsor N. K., "Theory of the Pulsed Electrothermal Thruster," AIAA Paper 1982-1952, Nov. 1982.

[3] Burton, R. L., Goldstein, S. A., Hilko, B. K., Tidman, D. A., and Winsor N. K., "Investigation of a Pulsed Electrothermal Thruster," GT Devices, Inc., NASA-CR-168266, Oct. 1983.

[4] Burton, R. L., Goldstein, S. A., Hilko, B. K., Tidman, D. A., and Winsor, N. K., "Experimental Investigation of the Pulsed Electrothermal (PET) Thruster," AIAA Paper 1984-1386, June 1984.

[5] Keidar, M. and Boyd, I. D., "Model of an Electrothermal Pulsed Plasma Thruster," Journal of Propulsion and Power. Vol. 19, No.3, 2003, pp. 424-430.

[6] Keidar, M. and Boyd, I. D., "Ablation Study in the Capillary Discharge of an Electrothermal Gun," Journal of Applied Physics, Vol. 99, No. 5, 2006, pp. 053301.1-053301.7.

[7] Admitsu, T. and Tahara H., "Experimental and Numerical Study of an Electrothermal Pulsed Thruster for Small Satellites," Vacuum, Vol. 80, No. 11-12, 2006, pp. 1223-1228.

[8] Painter, L. R., Arakawa, E. T., Williams, M. W., and Ashley, J. C., "Optical Properties of Polyethylene: Measurement and Applications," Radiation Research, Vol. 83, 1980, pp. 1-18.

[9] Ashok, J. and Birch, J. R., "Polyethylene $(C_2H_4)n$," Handbook of Optical Constants of Solids II, Academic Press, 1981.

[10] Emanuel, G., "Gasdynamics: Theory and Applications," AIAA Education Series, AIAA, New York, 1986.

[11] Anisimov, S. I., "Vaporization of Metal Absorbing Laser Radiation," Soviet Physics Journal of Experimental and Theoretical Physics, Vol. 27, No. 1, 1968, pp. 182-183.

[12] Keidar, M., Boyd, I. D., and Beilis I.I, "On the Model of Teflon Ablation in a Ablation-Controlled Discharge," Journal of Physics D: Applied Physics, Vol. 34, 2001, pp. 1675-1677.

[13] Pekker L., Keidar M., and Cambier J.-L., "Effect of Thermal Conductivity on the Knudsen Layer at Ablative Surfaces," Journal of Applied Physics, Vol. 103, 2008, pp. 034906.